International Journal of Biological Macromolecules 277 (2024) 134390

Contents lists available at ScienceDirect

International Journal of Biological Macromolecules

journal homepage: www.elsevier.com/locate/ijbiomac

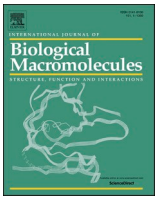

Structural studies of KCTD1 and its disease-causing mutant P20S provide insights into the protein function and misfunction

Nicole Balasco [a,1], Alessia Ruggiero [a,1], Giovanni Smaldone [c], Giovanni Pecoraro [c], Luigi Coppola [c], Luciano Pirone [b], Emilia M. Pedone [b], Luciana Esposito [b], Rita Berisio [b,*], Luigi Vitagliano [b,*]

[a] Institute of Molecular Biology and Pathology, CNR c/o Department Chemistry, Sapienza University of Rome, 00185 Rome, Italy
[b] Institute of Biostructures and Bioimaging, CNR, 80131 Naples, Italy
[c] IRCCS SYNLAB SDN, 80143 Naples, Italy

ARTICLE INFO

Keywords:
KCTD proteins
Scalp-ear-nipple syndrome
Domain swapping

ABSTRACT

Members of the KCTD protein family play key roles in fundamental physio-pathological processes including cancer, neurodevelopmental/neuropsychiatric, and genetic diseases. Here, we report the crystal structure of the KCTD1 P20S mutant, which causes the scalp-ear-nipple syndrome, and molecular dynamics (MD) data on the wild-type protein. Surprisingly, the structure unravels that the N-terminal region, which precedes the BTB domain (preBTB) and bears the disease-associated mutation, adopts a folded polyproline II (PPII) state. The KCTD1 pentamer is characterized by an intricate architecture in which the different subunits mutually exchange domains to generate a closed domain swapping motif. Indeed, the BTB of each chain makes peculiar contacts with the preBTB and the C-terminal domain (CTD) of an adjacent chain. The BTB-preBTB interaction consists of a PPII-PPII recognition motif whereas the BTB-CTD contacts are mediated by an unusual (+/−) helix discontinuous association. The inspection of the protein structure, along with the data emerged from the MD simulations, provides an explanation of the pathogenicity of the P20S mutation and unravels the role of the BTB-preBTB interaction in the insurgence of the disease. Finally, the presence of potassium bound to the central cavity of the CTD pentameric assembly provides insights into the role of KCTD1 in metal homeostasis.

1. Introduction

KCTD (K-potassium channel tetramerization domain-containing proteins) constitutes a class of emerging proteins that are involved in key physiopathological processes. The common element of this protein family is the presence, at the N-terminal region of all members, of a BTB domain [1] that presents a significant similarity with the tetramerization domain of the Kv4.2 potassium channels [2]. However, despite this similarity, there is no evidence that KCTD proteins, with the possible exception of KCNRG [2], may be involved in the potassium transport. An increasing number of independent studies carried out in the last decade have demonstrated that dysregulations of these proteins have been detected in the etiology of many diversified pathological states, including cancer [3,4], neurodevelopmental/neuropsychiatric [5], and genetic diseases [6–12]. For many years, a full understanding of the functionality of these proteins has been hampered by the paucity of related atomic-level structural data [13–15]. This scenario has rapidly changed in the last few years through the combination of experimental structural studies [16–20] and approaches based on machine-learning techniques [21–23]. These studies have provided a plausible global view of the structural features of these proteins and their interaction with some important biological partners. Based on these predictive studies, it has been shown that even the C-terminal domains (CTD) of these proteins, which were believed to be independent and evolutionary distinct modules, share some significant structural similarities throughout the family [21].

Structure-based clustering based on the similarity of the CTD domains has highlighted the segregation of two groups of the family (cluster 1A - KCTD8/KCTD12/KCTD16 and cluster 1B - KCTD1/KCTD15) that are not involved in protein ubiquitination/degradation.

* Corresponding authors.
E-mail addresses: rita.berisio@cnr.it (R. Berisio), luigi.vitagliano@cnr.it (L. Vitagliano).
[1] These authors contributed equally to this work.

https://doi.org/10.1016/j.ijbiomac.2024.134390
Received 19 June 2024; Received in revised form 18 July 2024; Accepted 30 July 2024
Available online 5 August 2024

Indeed, members of these two clusters do not bind Cullin 3 (CUL3), a common KCTD partner in protein ubiquitination/degradation [14,23–25]. While insightful structural and functional studies have provided important clues on the mechanism of action of cluster 1A members [16,26–28], clear structure/function relationships have not yet been established for KCTD1 and its close homolog KCTD15. Several literature reports have clearly demonstrated that the close homologs KCTD1 and KCTD15 recapitulate at a smaller scale the peculiar functional diversification of the KCTD family, due to their involvement in quite different biological processes. Indeed, it has been shown that dysregulations of these proteins are linked to neurodevelopmental disorders [5,12,29,30], obesity [31–33], cancer [3,34–40], and genetic diseases [6,7,12,41,42]. Notably, KCTD1 and KCTD15 mutations have been associated with scalp-ear-nipple syndrome (SENS), aplasia cutis congenita, kidney fibrosis, and cardiac outflow tract abnormalities ([12] and references therein). We and others have recently shown that the two proteins cooperate by forming functional heterocomplexes [12]. Although these disease-causing mutations are generally located in the folded regions of the KCTD1 protein [6,41], somehow surprisingly, one of them Pro20Ser is located in the presumably unfolded N-terminal region that precedes the BTB domain (preBTB).

To gain insights into the intricate role of the KCTD1 protein in different physiopathological contexts, we here present the crystal structure of the full-length disease-causing mutant P20S. The global pentameric structure of the protein presents an intricate architecture in which adjacent chains exchange the entire BTB domain to generate a closed domain swapping [43,44]. Uncommon interactions such as helix-helix discontinuous association and intermolecular PPII/PPII recognition domains characterize the interdomain contacts. The combination of these experimental data with computational studies provides a clear explanation of the puzzling pathogenicity of the P20S KCTD1 mutation. More importantly, the presence of a potassium ion bound to the central cavity of the CTD pentameric assembly provides insights into the role of KCTD1 and the other members of the family in metal homeostasis. Finally, we also describe the predicted model for a long-form of the protein which is conjugated with a Crypton transposon [45].

2. Materials and methods

2.1. Protein sample preparation

The KCTD1 protein used in this study includes residues 1–257 of the entire protein sequence (UniProtKB Q719H9) bearing the Pro20Ser mutation (KCTD1^{P20S}). The corresponding encoding sequence was cloned into the pETM-11 expression vector to produce an N-terminal cleavable His-tag protein.

2.2. Protein expression, purification, and crystallization

The Se-Met derivative of KCTD1^{P20S} was expressed in *E. coli* Rosetta (DE3)2 cells in 1 L of minimal media (M9) enriched with the following components: 0.4 % (*w/v*) glucose, 1 mM $MgSO_4$, 0.1 mM $CaCl_2$, 50 μg/mL ampicillin, 33 chloramphenicol, 100 μg/mL thiamine at 37 °C. After reaching an OD_{600} of 0.7, an amino acid mix (50 μg/mL of Ile, Leu, and Val and 100 μg/mL of Phe, Thr, and Lys) was added to the bacterial culture. After equilibration, 60 μg/mL of seleno-L-methionine was added and the induction was performed by adding 0.5 mM IPTG. Labeled and unlabelled KCTD1^{P20S} proteins were purified by coupling two consecutive chromatographic steps on the soluble bacterial lysate. The first step was carried out by using Ni-NTA affinity resin (Qiagen), then pooled fractions, containing KCTD1^{P20S} protein, were concentrated and loaded on the size-exclusion chromatography on S200 10/30 column equilibrated in 50 mM Tris-HCl, 150 mM NaCl, 5 % (*v/v*) glycerol, 0.01 % (*w/v*) CHAPS and 2 mM DTT (pH 7.8) The homogeneity of the protein was evaluated by SDS–PAGE analysis. The molecular mass of the purified protein was checked by mass spectrometry and no proteolysis of the protein was detected. Crystallization trials were performed by using the hanging-drop method at 293 K. After a preliminary screening of the crystallization conditions using different crystallization screens (Crystal Screen I and II, Index, Hampton Research), we were able to grow good quality crystals in 1.8 M sodium chloride, 0.1 M sodium phosphate monobasic monohydrate, 0.1 M potassium phosphate monobasic, and 0.1 M Mes monohydrate (pH 6.5) with a protein concentration of 4–6 mg/mL. Moreover, a further optimization of crystallization conditions was achieved using 0.2 M of sodium thiocyanate as an additive (Additive Formulation, Hampton Research) into the protein-precipitant drop. Good diffraction crystals were obtained for both Se-Met labeled and unlabelled KCTD1^{P20S} proteins.

2.3. Data collection and processing

Diffraction data for the Se-Met derivatives of KCTD1^{P20S} were collected at the ID30B synchrotron beamline at European Synchrotron Radiation Facility ESRF in Grenoble (France) at 100 K. Cryoprotection of the crystals was achieved by a fast soaking in a solution containing glycerol to a final concentration of 14 % (*v/v*). Anomalous diffraction data were collected at the peak of absorption of the selenium (0.979 Å). The crystals belong to the space group $P2_1$ (Table 1).

2.4. Structure solution and refinement

The data were processed using the program XDS and the automated protocol available at ESRF (Table 1). The structure of KCTD1^{P20S} was solved by Single Anomalous Dispersion (SAD) techniques using the automated procedures implemented at ESRF and the Phenix suite [46]. Crystallographic refinement of the structure of KCTD1^{P20S} was carried out against 95 % of the measured data using the CCP4i program [47]. The remaining 5 % of the observed data, which was randomly selected, was used in R-free calculations to monitor the progress of refinement. The refinement was performed using the programs Phenix and Refmac5 [48]. The refinement runs were followed by manual intervention using the molecular graphic program Coot [49], to correct minor errors in the position of the side chains. The inspection of the electron density in the cavity of the CTD domain revealed the presence of a metal ion coordinated by the carbonyl oxygens of residue Gly222 of the five protein chains. Considering the presence in the crystallization medium of both sodium and potassium, these ions were tentatively modelled in the cavity. The inspection of the metal-oxygen distances and of the B factor distributions indicated that the potassium ion is better suited for this coordination site as also suggested by the CheckMyMetal (CMM) server [50]. The stereochemical parameters of the refined structure (Table 2)

Table 1
X-ray data collection statistics for KCTD1^{P20S}.

Crystal data	
Space group	$P2_1$
Unit-cell parameters	
a, b, c (Å)	68.1, 96.0, 116.8
α, β, γ (°)	90.0, 98.2, 90.0
Data processing	
Resolution range (Å)	15.0–2.7
No. of unique reflections	52,034
No. of observations	175,801
Redundancy	3.4
Completeness (%)	99.6
$CC_{1/2}$	0.995
I/σ (I)	6.8
Rmerge (within I+/I-)	0.080
Rmerge (all I+ and I-)	0.106
Rpim (within I+/I-)	0.079
Rpim (all I+ and I-)	0.068

Table 2
Refinement statistics for KCTD1^{P20S}.

Refinement results	
R/R_{free} (%)	19.4/24.3
No. of molecules	
No. of residues	1062
No. of water molecules	82
RMSD from ideal values	
Bond lengths (Å)	0.006
Bond angles (°)	0.944
Average B-factors	
All atoms (Å^2)	80.0
Ramachandran plot statistics	
Favored (%)	92.5
Allowed (%)	7.1
Outliers (%)	0.4

are in close agreement with those obtained for well-refined protein structures at 2.7 Å resolution as highlighted by the program PROCHECK. In particular, 92.5 % of the residues are located in the favored regions of the Ramachandran plot. The stereochemistry of the model has also been evaluated by using an innovative approach based on the monitoring of the variability of subtle details of the peptide geometry including the NC$^{\alpha}$C bond angle and the Δω deviation from the peptide bond planarity [51,52]. To avoid any bias, this analysis was performed on a model refined using the stereochemical libraries of Phenix not considering the conformational dependence of the geometrical parameters. The results indicate that the variability of most parameters well follows the one detected in high-resolution protein structures (Supplementary Table S1 and Fig. S1). The final model was refined using the option CDL (conformation-dependent libraries) of Phenix. Atomic coordinates of KCTD1^{P20S} have been deposited in the PDB with 9FQ1 identification code.

2.5. AlphaFold predictions

Predictions of structural models were carried out using the AlphaFold (AF) v2.0 algorithm as implemented on the Colab server (https://colab.research.google.com/github/sokrypton/ColabFold/blob/main/AlphaFold2.ipynb) [53].

Predictions were carried out without considering any homologous experimental template (template_mode: none) and with three as the number of recycles and using AlphaFold-multimer v2. The best-predicted model (rank 1) out of the five computed by AF is considered. The reliability of the AF predictions was assessed by analyzing the Local Distance Difference Test (LDDT) score and the Predicted Aligned Error (PAE) matrices reported for each predicted structure.

2.6. Molecular dynamics simulations

Fully atomistic Molecular Dynamics (MD) simulations were performed on the KCTD1 pentamer using the GROMACS software (version 2022.3) with the Amber99sb all-atom force field [54]. Both the wild-type (predicted model by AF) and its P20S mutant here reported (PDB ID: 9FQ1) were considered as starting models. The protein models were solvated in triclinic boxes with TIP3P water molecules and neutralized with twenty sodium counterions (ionic strength of ~0.015 M). A 10 Å cut-off was applied for Lennard–Jones interactions whereas the Particle Mesh Ewald (PME) method (0.16 nm grid spacing) was used for the electrostatic interactions [55]. Bond lengths were constrained using the LINCS algorithm [56]. Systems were energy minimized with the steepest descent method for 50,000 steps, and subsequently equilibrated in two phases. The temperature was raised to 300 K in 500 ps (NVT ensemble), and then the pressure was equilibrated at 1 atm in 500 ps (NpT ensemble). The Velocity Rescaling and Parrinello−Rahman algorithms were applied to control temperature and pressure, respectively. Two replicas of 100 ns for each system were conducted at a constant temperature (300 K) and pressure (1 atm) with an integration time step of 2 fs. Structural analyses of the MD trajectories were carried out using GROMACS tools and the Visual Molecular Dynamics (VMD) program [57]. Figures of structural models and plots were obtained using the PyMOL molecular visualization program and Xmgrace v50125, respectively.

3. Results

3.1. Structural characterization of the disease-causing mutant P20S of KCTD1

To gain insights into the multiple biological roles of KCTD1, we undertook a structural characterization of the full-length protein (residues 1–257). All the attempts to grow crystals suitable for crystallographic investigations of the wild-type protein were unsuccessful. On the other hand, crystals amenable to structural studies were obtained for the full-length form of the disease-causing mutant P20S (KCTD1^{P20S}). While this investigation was in progress, a structure of a truncated form (residues 28–257) of KCTD1 was reported in the Protein Data Bank (PDB) (ID 6S4L - doi:https://doi.org/10.2210/pdb6S4L/pdb) with no publication hitherto associated. In the following paragraphs, a top-down description of the KCTD1^{P20S} structure is reported also in comparison with the previously reported 6S4L PDB structure and the AlphaFold here predicted models.

3.1.1. The intricate architecture of the KCTD1 pentamer: evidence for a close domain swapping

Despite the moderate resolution of the present study (2.7 Å), the electron density is well-defined for most of the protein residues. The disordered residues with no detectable electron densities correspond to the terminal regions (residues 1–18 and 242–257) and the loop 177–186. The inspection of the electron density also discloses structured regions at the N-terminal side of the BTB domain (preBTB), expected to be fully disordered. A well-defined density for the region 19–29 characterizes three chains, whereas the preBTB region is fully disordered in the other two chains (Supplementary Fig. S2).

The global structure of the KCTD1^{P20S} pentamer is characterized by an intricate architecture in which each of its folded elements, i.e., preBTB (residues 1–29), BTB (residues 30–133), and CTD (residues 139–239), establishes strong inter- rather than intra-subunit interactions. Indeed, the individual subunits mutually exchange domains to generate a closed pentameric 3D-domain swapping motif (Fig. 1). The swapping element is the BTB domain, as this motif is exchanged by two adjacent chains. In this swapping motif, the BTB and the preBTB/CTD domains of one chain interact with two distinct adjacent chains (Fig. 1B). Although 3D-domain swapping is a widespread phenomenon in protein three-dimensional structures [44,58], the structural complexity of KCTD1 in terms of the oligomeric state and the size of the swapped element is rather unusual. A deep inspection of the interactions that stabilize the 3D-domain swapped pentamer of KCTD1^{P20S} indicates that both the preBTB/BTB and BTB/CTD interfaces rely on intriguing and somehow unusual association modes. As anticipated above, the preBTB domain, which was expected to be unfolded and was even removed in a previous crystallographic study of the isolated BTB domain of KCTD1 to facilitate the crystallization [14], is in part well-folded in KCTD1^{P20S}. Indeed, in three out of the five chains of the pentamer, the preBTB region embedding residues 20–25 adopts a polyproline II (PPII) structure which protrudes to a hosting cavity of the BTB domain of an adjacent chain (Figs. S2 and 2). Indeed, the (φ,ψ) values of the residues of this region in the chains in which they are ordered well agree

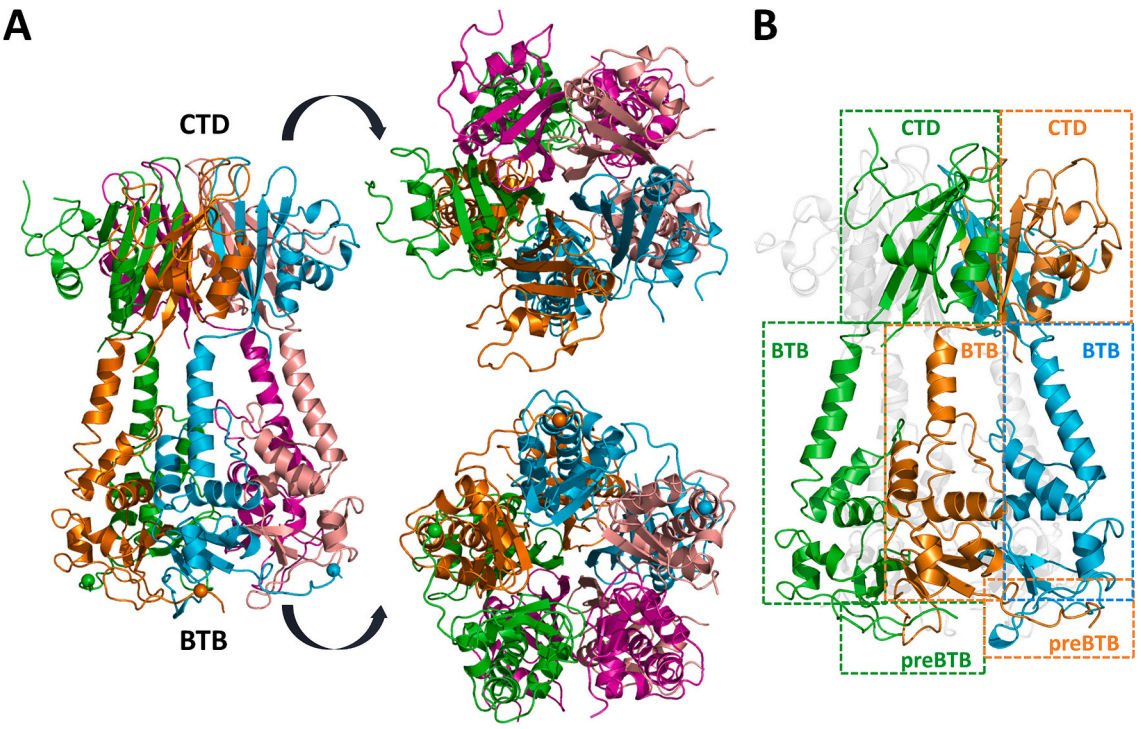

Fig. 1. The intricate architecture of the disease-causing mutant P20S of KCTD1. Different views of the pentamer colored by chain (A), the curved arrows indicate the rotation of 90 degrees in opposite directions around the horizontal axis. The position 20 bearing the P20S mutation is shown as a sphere. Schematic representation of KCTD1^{P20S} closed 3D-domain swapping motif (B).

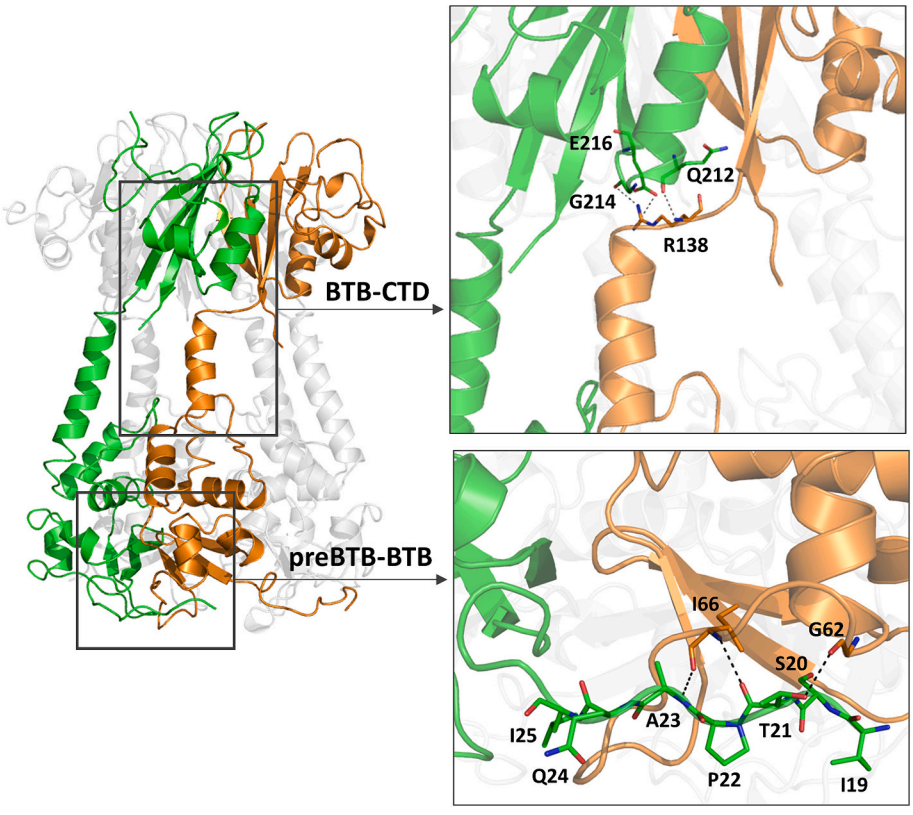

Fig. 2. Interdomain (preBTB-BTB and BTB-CTD) interfaces that stabilize the domain-swapped pentamer in the crystal structure of KCTD1^{P20S}. Residues of the preBTB domain and those involved in hydrogen bonding interactions at the interdomain interfaces are shown as sticks.

(Supplementary Table S2) with the values expected for PPII helices [59]. The preBTB/BTB interface is stabilized by three hydrogen-bonding interactions that involve the main chain of Thr21 (O atom) and Ala23 (N atom) of the PPII fragment and both the N and O atoms of Ile66 on the BTB domain (Fig. 2). The interaction is further stabilized by a hydrogen bond formed by the Thr21 side chain with the oxygen atom of the residue Gly62. The analysis of the PDB models of KCTD1 (PDB ID 6S4L) and its BTB domain (PDB ID 5BXB), in which the preBTB region was truncated, shows that the structure of the PPII recognition motif on the BTB of these models is virtually identical to the one here detected. This suggests that this BTB cavity is appropriately pre-organized to anchor the PPII helix. It is important to note that the SENS-causing Pro20Ser mutation that characterizes the present structure likely reduces the PPII propensity of the preBTB region, likely destabilizing its interaction with the BTB domain (see below the MD studies). A discontinuous helix formed by the helices 118–136 of the BTB domain and 203–213 of the CTD domain characterizes the inter-molecular BTB-CTD interface (Fig. 2). The interaction is stabilized by the peculiar juxtaposition of negative and positive poles of the dipoles of the two helices (+/− dipolar association). Indeed, the negative pole of the C-terminus of the BTB helix is associated with the positively charged N-terminus of the helix of the CTD. The BTB-CTD interface is further stabilized by interactions made by the charged residues that typically counterbalance the charge of the helix dipoles. In this scenario, strong electrostatic interactions are established by the side chains of Arg138 and Glu216 (Fig. 2). Moreover, the side chain of Arg138 interacts with the O atom of Gly214. Finally, a main chain-main chain hydrogen bond is formed between Arg138 (N atom) and Gln212 (O atom). Similar BTB-CTD interactions are present in the truncated form of the protein deposited in the PDB (PDB ID 6S4L) (Fig. S3A).

3.1.2. The CTD domain: fold and metal binding

In line with the previous AlphaFold prediction and with the PDB structure of the truncated form of KCTD1 (PDB ID 6S4L), five copies of the CTD domain assemble to form a pentameric structure that resembles the common β-propeller fold (Fig. 3A). However, the KCTD1 CTD pentameric structure presents two main distinctive features when compared to canonical β-propellers: (a) the contribution of five distinct subunits to generate a fold that is typically formed by a single polypeptide chain, (b) the presence of two helices *per* subunit in addition to the β-structure, and (c) a reduced size of the central channel. Moreover, the main chain hydrogen bond donors and acceptors of the edge β-strands, which delimitate the internal channel of the CTD pentamer, are fully exposed and not involved in hydrogen bonding interactions. Considering the intrinsic stickiness of the exposed β-strands and the limited size of the side chains of the residues that compose the strand (Gly, Val, Ser, Cys), it is not surprising that different chemical species are bound to the internal channel formed by the assembly of the CTDs. The inspection of the electron density shows the binding of two phosphate groups, a potassium ion, and a water molecule in the central channel of the pentamer (Fig. 3B). The position in the channel is dictated by hydrogen bonding interactions with the backbone atoms of the exposed edge β-strands. In particular, the five backbone oxygen atoms of Gly222 form a plane that coordinates the potassium ion. In the channel, the average metal-oxygen distance is ~2.6 Å which is in line with the expected ligand-potassium coordination distances [60]. Moreover, the observed similarity of the B factors of the potassium and its protein coordination atoms also indicates that this metal occupies the coordination site (see Material and Methods for details).

The coordination of the metal is completed, in the apical positions by the oxygen atom of a phosphate group (p1, K^+-O distance of 3.2 Å) and a water molecule (K^+-O distance of 3.8 Å). A second phosphate group (p2) directly bound to p1 closes the channel (Fig. 3B).

3.2. The intriguing ability of AlphaFold to predict the structure of KCTD1 and its long isoform

The determination of the crystallographic structure of KCTD1^{P20S} provides the opportunity to assess the reliability of a previously reported predicted AF model of KCTD1 and to generate models of the wild-type protein as well as of its long isoform (865 residues – UniProtKB A0A2U3U043) that also contains a tyrosine recombinase (YR) element of Crypton DNA transposons.

In a comprehensive analysis of putative three-dimensional structures of all members of the KCTD proteins, we generated the pentameric AF structure of KCTD1 regions that were expected to be folded (BTB + CTD) [22]. In line with the well-known ability of the algorithm to predict protein structures, for the protein portion embodying the BTB and CTD

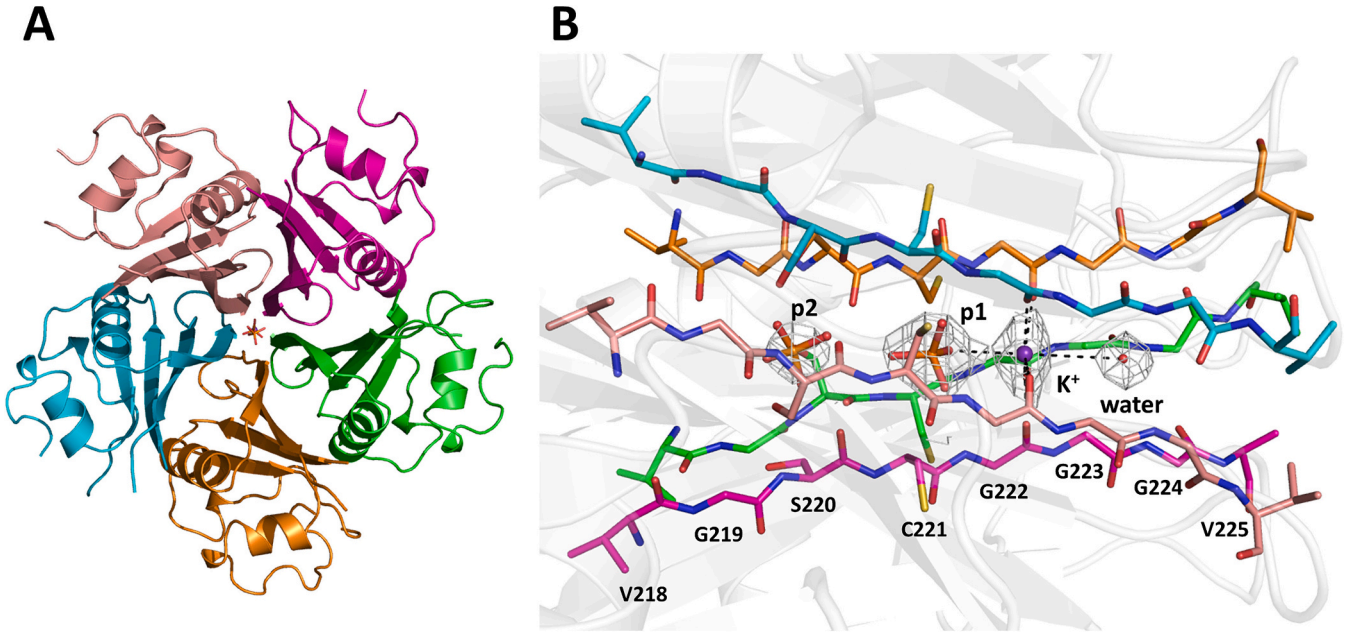

Fig. 3. CTD domain of KCTD1^{P20S}. Top view of the CTD colored by chain in the crystal structure of KCTD1^{P20S} (A). The |2Fo-Fc| electron density of the ligands (a potassium ion K^+, a water molecule, and two phosphate groups denoted as p1 and p2) in the channel is shown as mesh at 1.3σ (B).

domains (residues 30–239), the AF model is very similar to the here described crystallographic one (RMSD deviation of 0.59 Å over 976 C^{α} atoms). The discovery that the preBTB region of the protein is folded and contributes to the pentamer stability prompted us to carry out predictions on the full-length wild-type variant of KCTD1. The generated AF model can capture, not only the BTB-CTD association mode but also the preBTB-BTB interactions (Fig. S3B). Even more surprising is the observation that the prediction of the structure of a single chain of KCTD1 provides the correct folding and orientation of the preBTB region observed in the crystal structure (Fig. S3C-D), despite the absence and an adjacent hosting BTB monomer. This finding may suggest that the BTB/preBTB orientation observed in the single chain could be a recurrent motif that the algorithm learned in the training process. However, attempts to interrogate structural databases using the preBTB region and its own BTB as the search fragment did not yield positive results.

In addition to the standard KCTD1 protein, which is made of 257 residues, four other isoforms have been reported (https://www.uniprot.org/uniprotkb/Q719H9/entry) and detected at the protein level. Two of them (UniProtKB J3QLL6 and J3KSG1) correspond to smaller portions (100 and 208 residues) of the canonical forms, while another (UniProtKB J3QRK1) is similar to the main isoform as it contains and lacks a few extra residues at the N-terminus and C-terminus, respectively (260 residues). On the other hand, the fourth isoform (UniProtKB A0A2U3U043), which is much longer containing 865 residues, embodies other functional domains in addition to the preBTB, BTB, and CTD ones. Indeed, it contains a DUF3504 domain which presents some sequence similarities with Cryptons, a unique class of DNA transposons using tyrosine recombinase [45]. Notably, this domain is not present in any of the KCTD15 isoforms. As no structural data is available for the DUF3504 domain, we analyzed the AF model of this long variant of KCTD1 (Fig. 4). The AF structure highlights the presence of two independent folded regions: the first (residues 167–470) including the DUF domain (residues 286–466), and the second (residues 609–865), located at the C-terminus, corresponding to the canonical isoform. The first structural region is composed of two folded domains (residues 170–273 and 286–466), which, although not physically interacting, present a relative orientation that is assessed as reliable by AF based on the predicted aligned error map (Fig. 4B). This puzzling observation may suggest that this is a preferential orientation of similar domains present in structural databases. As shown in Fig. 4C, the relative orientation of the two domains of this folded unit of the long form of KCTD1 closely resembles that found in a DNA complex of the Cre recombinase (PDB ID 5CRX) [61], which is a member of the integrase family, despite the absence of any sequence similarity between the proteins. Evidently, the reliability of the orientation of the two domains in the KCTD structure that emerged from the AF self-assessment derives from the presence in the PDB of related situations. This finding demonstrates that AF predictions may provide, in addition to reliable predictions of the protein folds and of direct protein-protein interactions, clues on the structural partnerships mediated by other biomolecules.

3.3. *Molecular dynamics simulations provide a dynamic view of the KCTD1 pentamer*

To gain further insights into KCTD1 functions and dysregulations, we performed atomistic MD simulations on the wild-type and the Pro20Ser mutant of the protein. As detailed in the Materials and methods section, we performed two replicas each for the wild-type and the mutant using the AF and the crystallographic structures, respectively, as the starting model.

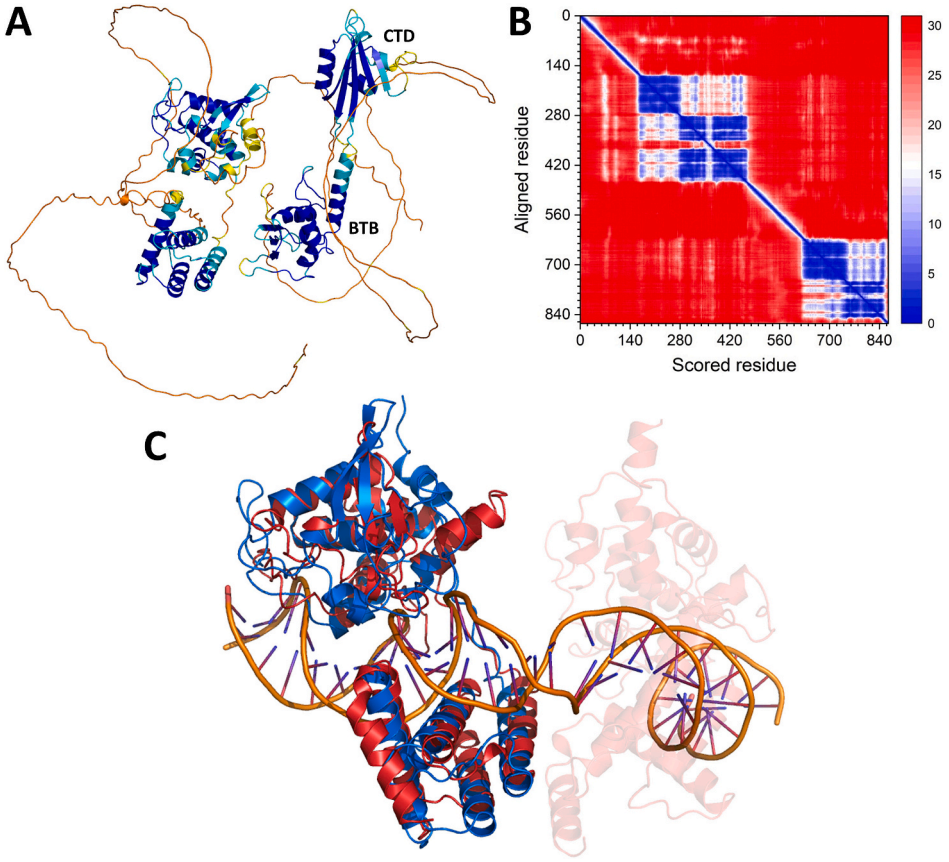

Fig. 4. AF predicted structure of the long isoform of human KCTD1 (UniProtKB A0A2U3U043). Cartoon representation (A) and PAE matrix (B) of the KCTD1 isoform colored according to the AF per-residue confidence metric (pLDDT). Structural alignment of the N-terminal region (residues 170-466) of the KCTD1 isoform (blue) with Recombinase cre (red, UniProtKB P06956, PDB ID 5CRX) (C). The structures superimpose with 2.9 Å RMSD over 246 C^{α} atoms.

As demonstrated by the structural indicators commonly used to monitor the trajectory of MD simulations, all replicas achieved stable states in the first 20 ns, with RMSD values of the trajectory structures *versus* the starting models mostly confined in the 1.5 to 2.0 Å range (Fig. S4). The stability of the MD structures was also corroborated by the analysis of other indicators such as secondary structure and gyration radius (data not shown). A comparative analysis of the MD data for the wild-type and the mutant highlights significant differences. The residue Pro20 of the wild-type KCTD1 almost uniquely adopts PPII conformations whereas Ser20 of the mutant frequently shifts between PPII and extended conformational states (Fig. S5). This behavior has consequences for the persistence of the interactions that stabilize the preBTB-BTB association. Although, in line with the crystallographic data and the AF predictions, these interactions are generally preserved, their conservation is higher in the wild-type compared to the mutant (Fig. 5). Indeed, the hydrogen bonds that stabilize the preBTB-BTB interface are more frequently broken in the mutant as demonstrated by the occurrence of large distances (>3.3 Å) between the donor and the acceptor. Collectively, these data indicate that the preBTB/BTB association is partially perturbed in the mutant with the likely destabilization of the pentameric assembly. The availability of MD simulations, which were carried out in water without the addition of potassium or phosphate ions that could interact with the protein, also provided us with the possibility to evaluate the intrinsic dynamics of the central channel of the CTD. Minimal variations of the channel are observed throughout the simulation, suggesting that the channel is pre-organized to anchor the ions in the positions we detected in the crystal structure (Fig. S6). The comparison of the channel dynamics in the wild-type and the Pro20Ser mutant highlights subtle but significant differences as its size appears to be smaller in the former. It can be surmised that the strong binding of the preBTB to the BTB region may produce long-distance effects and tighten the association of the chains in the CTD.

4. Discussion

KCTDs represent a protein family whose members play an active role in several important physiopathological processes [3–12]. Despite this, the definition of the mechanisms underlying their many functions is still limited. Here we gained detailed structural and dynamic data on one of the most important members of the family, KCTD1, by combining crystallographic analyses, prediction studies, and molecular dynamics simulations. As delineated in the following paragraphs the analysis of the global and local structure of the KCTD1^{P20S} mutant provides insights into the mechanism underlying the role of the protein in both pathological and physiological processes.

The global architecture of the protein is characterized by an intricate association of five subunits in a pentameric structure whereby each of the three protein subunits (preBTB, BTB, and CTD) contributes to the pentamer stability by making intermolecular, rather than intramolecular, interactions (Figs. 1 and 2). The mutual exchange of structural units among the different subunits generates an unusual pentameric closed 3D-domain swapping. Particularly interesting is the association, mediated by the domain swapping, of the preBTB region with the BTB domain, which is a well-characterized domain frequently deputed to hetero- and self-interactions [62]. Recent investigations have demonstrated that, in addition to oligomers, BTB domains may form functional polymeric species by exploiting newly discovered interfaces [63,64]. The detection of domain swapping between interacting BTBs here detected in the KCTD1 structure further expands the known associating modes that these versatile domains use to oligomerize.

The peculiar association of the five chains in KCTD1^{P20S} is not just a structural curiosity but holds important consequences for the mechanism of the pentamer (de)stabilization, as modifications inside a single unit are likely to affect interchain rather than intrachain interactions. This observation is suited to explain on a structural basis the effects induced by the mutation of Pro20 to Ser, which has been reported as a causative event of the SENS [6]. Data here presented show that this

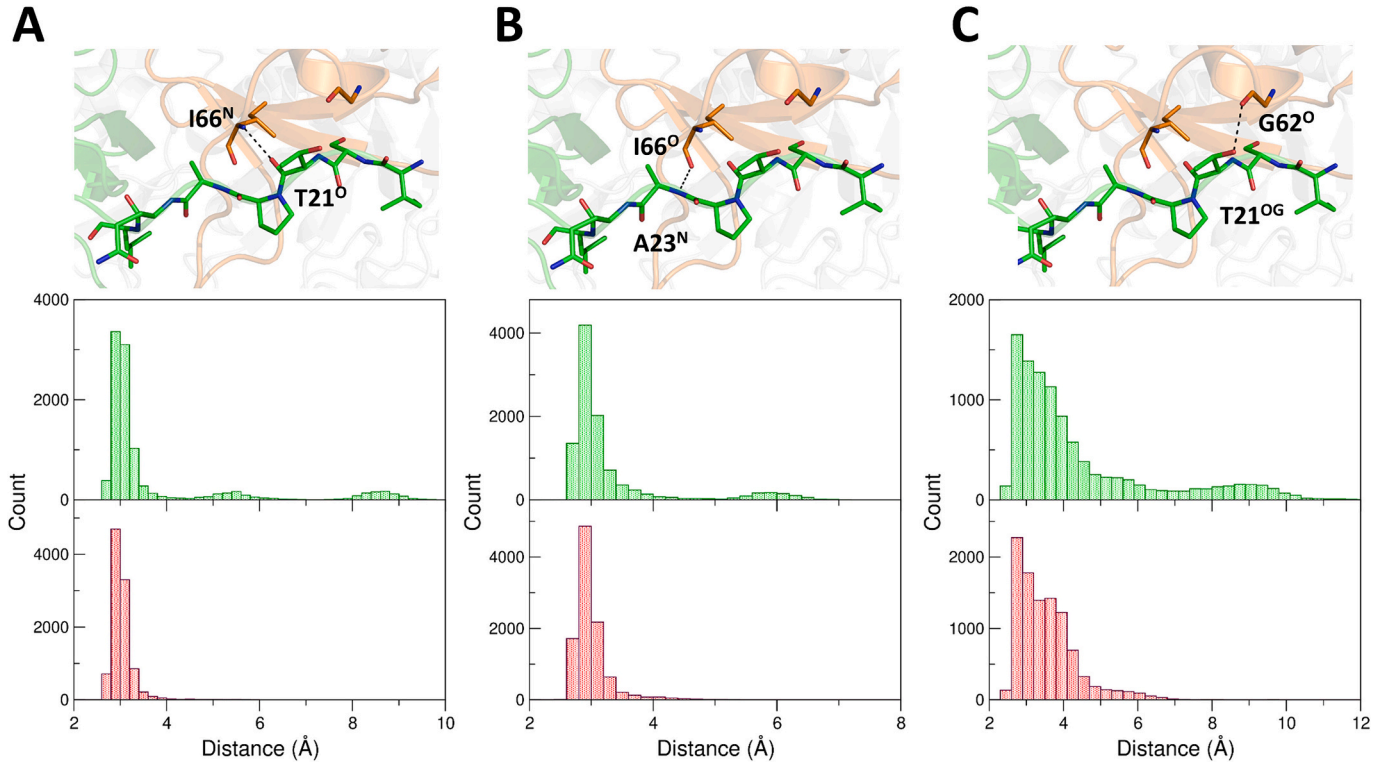

Fig. 5. PreBTB-BTB interaction in the MD simulations. Comparative analysis of the distances that stabilize the preBTB-BTB interdomain contacts in the MD simulations of KCTD1^{P20S} (green) and KCTD1 wild-type (red): T21O-I66N (A), A23N-I66O (B), and T21OG-G62O (C). (For interpretation of the references to colour in this figure legend, the reader is referred to the web version of this article.)

mutation site does not belong, as previously believed, to an unfolded region but it is embedded in a PPII motif that is deeply involved in intermolecular interactions that stabilize the global pentameric assembly. As corroborated by MD simulations, the substitution of the proline weakens the interaction of the PPII region with the BTB of an adjacent chain and destabilizes the global protein structure. This consideration is in perfect agreement with the observation of a partial destabilization of the KCTD1 structure induced by this mutation or by the truncation of the N-terminal preBTB region of the protein. This finding also explains the observed destabilization of KCTD1^{P20S} pentamer that likely exposes aggregation-prone regions. Indeed, it has been demonstrated that the mutant is endowed with a higher propensity to form amyloid-like aggregates that make it unable to bind its functional partner TFAP2A [41]. This mechanism well explains the dominant character of the P20S mutation that causes SENS also in heterozygotic individuals. Indeed, the amyloid-like aggregates formed by the P20S KCTD1 variant may serve as a template for the aggregation of the wild-type proteins present in these patients. This hypothesis is corroborated by the finding that disease-associated KCTD1 variants form amyloid-like assemblies both in vitro [41] and in cell systems [12,65] and favor the aggregation of the wild-type protein.

The observation that the preBTB region plays an active role in the stabilization of the protein goes well beyond the Pro20Ser mutation. Indeed, other disease-related mutations affect the preBTB/BTB recognition sites, involving, in particular, residues Gly62 and Ile66 that play a direct role in the interaction (Fig. S7) [6,66]. Interestingly, with the same conceptual framework, the pathological phenotype detected in heterozygous mice bearing the KCTD1 mutation Ile27Asn (residue 19 in the human sequence) can be ascribed to the destabilization of this interaction [67]. It is worth mentioning that a similar structural arrangement, with the preBTB playing an active role in the pentamer interactions, is predicted also for KCTD15 (Fig. S8), a close homolog that cross-acts with KCTD1 both physiologically and pathologically [7]. Regarding other mutations putatively associated with pathological states, it has been recently reported that mutations in the C-terminal region of the protein (Arg241Gln and Pro243Ser) may be associated with dental anomalies [68]. The authors suggested that these mutations could alter the ability of the protein to establish biological partnerships and/or undergo posttranslational modifications. It is worth noting that this region does not assume a rigid structure in the crystallographic model of the protein (PDB ID 6S4L) and it is not reliable in the AlphaFold 2 model (Fig. S3C). On the other hand, its predicted structure using the newly released AlphaFold 3 reliably suggests that this region folds in a PPII motif that is inserted in the cavity formed by the C-terminal helices of the BTB domain of adjacent chains. In this scenario, the two mutations destabilize these interactions either by eliminating the contacts formed by Arg241 or by undermining the PPII motif (Fig. S9).

In more general terms, KCTD1 functionality is extremely sensitive to amino acid replacements. Indeed, as indicated by the predictions reported in the AlphaMissense database [69], except for a limited number of residues, the vast majority of replacements are likely to induce pathological effects (Fig. S10). This is also detected for the preBTB PPII region. Notably, the percentage of amino acid replacements in KCTD1 that are predicted to be pathological by AlphaMissense is 76.5. This value is particularly high if compared to the global percentage (32 %) of predicted pathological replacement in the human proteome by the same algorithm [69]. This observation well agrees with the remarkable conservation of the protein during the evolution. The mouse and human sequences are 100 % identical (Table S3), a rather uncommon situation detected in only 2.3 % of cases in large-scale statistical comparisons [70]. Remarkable similarities are observed also in comparison with more distant organisms (Table S3). The extreme susceptibility of KCTD1 to amino acid replacements is likely due to its intricate architecture and propensity to aggregate [12,41,71].

The CTD domain, which adopts a structure that constitutes a variation of the common β-propeller fold (Fig. 3), is similar to that previously reported in the truncated forms of the protein (PDB ID 6S4L). The structure of the CTD pentamer has close analogies with that exhibited by the GTP cyclohydrolase 1 feedback regulatory protein (GTPCH-GFRP) (Fig. S11A) [72]. Although global alignments of the sequence of GTPCH-GFRP with that of KCTD1 do not yield remarkable similarities, the fold of the two proteins is similar as demonstrated by the RMSD value (5.8 Å RMSD over 305 C^{α} atoms of the five chains) obtained upon their overlap (right side of Fig. S11A). Nevertheless, a significant sequence identity is detected for the exposed β-strand that delimitates the channel as small residues (Gly, Ser, Val) are predominant in both proteins, thus indicating a common evolutionary origin of the two proteins. Despite the striking structural analogy of KCTD1 and GTPCH-GFRP, only water molecules were found in the internal channel of the regulatory protein (Fig. S11B), notwithstanding the presence of potassium ions in the crystallization medium. The fold of the KCTD1 CTD domain has also significant similarities with the paraflagellar rod component Q4D6Q6, a kinetoplastid-specific protein from Trypanosoma cruzi (Fig. S12) [73]. Although the paraflagellar rod component adopts a tetrameric state, its central channel is occupied by positive and negative ions, similar to KCTD1 (Fig. S12A). Moreover, the search for structural homologs of the CTD domain was conducted also considering the ensemble of all human proteins, whose structure was predicted by AF, using the DALI server [74]. This survey uncovered that the protein Raftlin-2 can adopt a similar structural organization. However, in this protein, a four-blade propeller formed by a single polypeptide chain is observed (Fig. S12B). Although the biological meaning of this similarity is yet to be disclosed, it nevertheless indicates that this type of structure may be achieved using either single or multiple subunits. As we previously anticipated using the predicted structures of KCTDs [22], the CTD domains of these proteins present significant analogies despite the marginal or absent sequence similarities between the members of different clusters. In line with these predictions, we here observe that some features of the propeller-like folding of the CTD of KCTD1 are present not only in the close homolog KCTD15 but also in distant KCTDs. In particular, the propeller-like fold with a solvent-exposed backbone of the edge strand is detected in other KCTDs (see Fig. S13 for some representative examples), although the degree of similarity is different when distinct members of the family are considered. Indeed, significant similarities are detected when KCTD1 is compared to KCTD12 (RMSD value of 2.5 Å over 325 C^{α} atoms) and KCTD5 (RMSD value of 8.1 Å over 188 C^{α} atoms), despite the smaller size of the CTD of the latter. In other cases (KCTD4 and KCNRG), only the global shape of the CTD domain is preserved.

In the crystallographic structure of KCTD1^{P20S} here determined, the central channel, which presents a funnel-like shape, is filled with different ions. The anchoring of these ions is assured by the exposure of the oxygen and the nitrogen backbone atoms of the edge strand which is generally composed of residues with small side chains (Gly, Val, Ser, Cys). Due to the fivefold symmetry of the channel, planes of pentamers formed by these hydrogen bond donors and acceptors may be identified. In KCTD1, the oxygen atom of Gly222 assures a planar penta-coordination of a potassium ion, in a manner that vaguely resembles that found in crown ethers. The coordination of the metal is completed by a phosphate group and a water molecule present in the funnel that limits its mobility (Fig. 3). It is worth mentioning that this coordination is similar to that observed for the calcium in calmodulin [75] and that this metal could be located in the channel with a suitable geometry without any steric hindrance (Fig. S14). Based on these observations and considerations, the central funnel of KCTD1 seems to be specifically designed to bind the potassium and likely other metals. The other ions or water molecules bound into the channel strongly limit the mobility of the metal, thus favoring its sequestration. The ability of KCTD1 to bind metals may be related to its role in metal homeostasis. The inspection of the structural models of KCTDs whose CTD is endowed with a propeller-like fold indicates that the funnel may have different sizes (Table S4). The data reported in the table indicate that KCTD1/KCTD15 presents the

narrowest funnels and a channel size that can directly bind metals. Rather narrow funnels are also formed by the KCTD proteins of the cluster 1A (KCTD8/KCTD12/KCTD16). For the other KCTDs, the putative binding of the metal would require a significant reduction of the funnel.

In conclusion, considering the importance of metals in neurodevelopmental and neurologic disorders, the finding that emerged in this study, that KCTD proteins are potentially able to bind metals, represents an intriguing hypothesis to be further investigated in the future. Recent studies showing that the effects of the KCTD5 downregulation in mice models may be mitigated by the addition of metal chelators go in the direction here proposed [76].

CRediT authorship contribution statement

Nicole Balasco: Writing – review & editing, Writing – original draft, Methodology, Investigation, Formal analysis. **Alessia Ruggiero:** Writing – review & editing, Methodology, Investigation. **Giovanni Pecoraro:** Writing – review & editing, Methodology, Investigation, Funding acquisition. **Luigi Coppola:** Writing – review & editing, Methodology. **Luciano Pirone:** Writing – review & editing, Investigation. **Emilia M. Pedone:** Writing – review & editing, Investigation. **Luciana Esposito:** Writing – review & editing, Formal analysis. **Rita Berisio:** Writing – review & editing, Validation, Formal analysis, Conceptualization. **Luigi Vitagliano:** Writing – review & editing, Writing – original draft, Validation, Funding acquisition, Formal analysis, Conceptualization.

Declaration of competing interest

The authors declare that they have no known competing financial interests or personal relationships that could have appeared to influence the work reported in this paper.

Acknowledgments

We would like to thank Giorgio Varriale, Maurizio Amendola, Massimiliano Mazzocchi, and Luca De Luca for their technical support. We acknowledge the CINECA award under the ISCRA initiative (ISCRA B project KCTD-CTD ID HP10BBY7W1 and ISCRA C project AF-Koli ID HP10C52U80), for the availability of high-performance computing resources and support. We acknowledge the European Synchrotron Radiation Facility (ESRF) for the provision of synchrotron radiation facilities and we would like to thank Andrew McCarthy for assistance and support in using beamline ID30B.

Funding

This work was supported by PNRR MUR – CN00000013 “National Centre for HPC, Big Data and Quantum Computing – Spoke 8” and by the Italian Ministry of Health (grant “Ricerca Corrente”).

Appendix A. Supplementary data

Supplementary data to this article can be found online at https://doi.org/10.1016/j.ijbiomac.2024.134390.

References

[1] P.J. Stogios, G.S. Downs, J.J. Jauhal, S.K. Nandra, G.G. Privé, Sequence and structural analysis of BTB domain proteins, Genome Biol. 6 (2005) R82, https://doi.org/10.1186/gb-2005-6-10-r82.

[2] M. Skoblov, A. Marakhonov, E. Marakasova, A. Guskova, V. Chandhoke, A. Birerdinc, A. Baranova, Protein partners of KCTD proteins provide insights about their functional roles in cell differentiation and vertebrate development, BioEssays 35 (2013) 586–596, https://doi.org/10.1002/bies.201300002.

[3] A. Angrisani, A. Di Fiore, E. De Smaele, M. Moretti, The emerging role of the KCTD proteins in cancer, Cell Commun. Signal 19 (2021) 56, https://doi.org/10.1186/s12964-021-00737-8.

[4] G. Canettieri, L. Di Marcotullio, A. Greco, S. Coni, L. Antonucci, P. Infante, L. Pietrosanti, E. De Smaele, E. Ferretti, E. Miele, M. Pelloni, G. De Simone, E. M. Pedone, P. Gallinari, A. Giorgi, C. Steinkühler, L. Vitagliano, C. Pedone, M. E. Schinin, I. Screpanti, A. Gulino, Histone deacetylase and Cullin3–RENKCTD11 ubiquitin ligase interplay regulates hedgehog signalling through Gli acetylation, Nat. Cell Biol. 12 (2010) 132–142, https://doi.org/10.1038/ncb2013.

[5] X. Teng, A. Aouacheria, L. Lionnard, K.A. Metz, L. Soane, A. Kamiya, J. M. Hardwick, *KCTD*: a new gene family involved in neurodevelopmental and neuropsychiatric disorders, CNS Neurosci. Ther. 25 (2019) 887–902, https://doi.org/10.1111/cns.13156.

[6] A.G. Marneros, A.E. Beck, E.H. Turner, M.J. McMillin, M.J. Edwards, M. Field, N. L. de Macena Sobreira, A.B.A. Perez, J.A.R. Fortes, A.K. Lampe, M.L. Giovannucci Uzielli, C.T. Gordon, G. Plessis, M. Le Merrer, J. Amiel, E. Reichenberger, K. M. Shively, F. Cerrato, B.I. Labow, H.K. Tabor, J.D. Smith, J. Shendure, D. A. Nickerson, M.J. Bamshad, Mutations in KCTD1 cause scalp-ear-nipple syndrome, Am. J. Hum. Genet. 92 (2013) 621–626, https://doi.org/10.1016/j.ajhg.2013.03.002.

[7] K.A. Miller, D.A. Cruz Walma, D.M. Pinkas, R.S. Tooze, J.C. Bufton, W. Richardson, C.E. Manning, A.E. Hunt, J. Cros, V. Hartill, M.J. Parker, S.J. McGowan, S.R. F. Twigg, R. Chalk, D. Staunton, D. Johnson, A.O.M. Wilkie, A.N. Bullock, BTB domain mutations perturbing KCTD15 oligomerisation cause a distinctive frontonasal dysplasia syndrome, J. Med. Genet. 61 (2024) 490–501, https://doi.org/10.1136/jmg-2023-109531.

[8] K.A. Metz, X. Teng, I. Coppens, H.M. Lamb, B.E. Wagner, J.A. Rosenfeld, X. Chen, Y. Zhang, H.J. Kim, M.E. Meadow, T.S. Wang, E.D. Haberlandt, G.W. Anderson, E. Leshinsky-Silver, W. Bi, T.C. Markello, M. Pratt, N. Makhseed, A. Garnica, N. R. Danylchuk, T.A. Burrow, P. Jayakar, D. McKnight, S. Agadi, H. Gbedawo, C. Stanley, M. Alber, I. Prehl, K. Pearlso, M.T. Ong, S.R. Mordekar, M.J. Parker, D. Crooks, P.B. Agrawal, G.T. Berry, T. Loddenkemper, Y. Yang, G.H.B. Maegawa, A. Aouacheria, J.G. Markle, J.A. Wohlschlegel, A.L. Hartman, J.M. Hardwick, *KCTD7* deficiency defines a distinct neurodegenerative disorder with a conserved autophagy-lysosome defect, Ann. Neurol. 84 (2018) 766–780, https://doi.org/10.1002/ana.25351.

[9] W. Wang, L. Su, L. Meng, J. He, C. Tan, D. Yi, D. Cheng, H. Zhang, G. Lu, J. Du, G. Lin, Q. Zhang, C. Tu, Y.-Q. Tan, Biallelic variants in *KCTD19* associated with male factor infertility and oligoasthenoteratozoospermia, Hum. Reprod. 38 (2023) 1399–1411, https://doi.org/10.1093/humrep/dead095.

[10] Y. Wang, H. Wang, C. Wang, Lysosomal dysfunction, autophagic defects, and CLN5 accumulation underlie the pathogenesis of KCTD7-mutated neuronal ceroid lipofuscinoses, Autophagy 19 (2023) 1876–1878, https://doi.org/10.1080/15548627.2022.2140882.

[11] M. Todisco, S. Gana, G. Cosentino, E. Errichiello, S. Arceri, M. Avenali, E. M. Valente, E. Alfonsi, KCTD17-related myoclonus-dystonia syndrome: clinical and electrophysiological findings of a patient with atypical late onset, Parkinsonism Relat. Disord. 78 (2020) 129–133, https://doi.org/10.1016/j.parkreldis.2020.07.026.

[12] J.R. Raymundo, H. Zhang, G. Smaldone, W. Zhu, K.E. Daly, B.J. Glennon, G. Pecoraro, M. Salvatore, W.A. Devine, C.W. Lo, L. Vitagliano, A.G. Marneros, KCTD1/KCTD15 complexes control ectodermal and neural crest cell functions, and their impairment causes aplasia cutis, J. Clin. Invest. 134 (2024) e174138, https://doi.org/10.1172/JCI174138.

[13] D.M. Pinkas, C.E. Sanvitale, J.C. Bufton, F.J. Sorrell, N. Solcan, R. Chalk, J. Doutch, A.N. Bullock, Structural complexity in the KCTD family of Cullin3-dependent E3 ubiquitin ligases, Biochem. J. 474 (2017) 3747–3761, https://doi.org/10.1042/BCJ20170527.

[14] A.X. Ji, A. Chu, T.K. Nielsen, S. Benlekbir, J.L. Rubinstein, G.G. Privé, Structural insights into KCTD protein assembly and Cullin3 recognition, J. Mol. Biol. 428 (2016) 92–107, https://doi.org/10.1016/j.jmb.2015.08.019.

[15] I.S. Dementieva, V. Tereshko, Z.A. McCrossan, E. Solomaha, D. Araki, C. Xu, N. Grigorieff, S.A.N. Goldstein, Pentameric assembly of potassium channel tetramerization domain-containing protein 5, J. Mol. Biol. 387 (2009) 175–191, https://doi.org/10.1016/j.jmb.2009.01.030.

[16] S. Zheng, N. Abreu, J. Levitz, A.C. Kruse, Structural basis for KCTD-mediated rapid desensitization of GABAB signalling, Nature 567 (2019) 127–131, https://doi.org/10.1038/s41586-019-0990-0.

[17] W. Jiang, W. Wang, Y. Kong, S. Zheng, Structural basis for the ubiquitination of G protein βγ subunits by KCTD5/Cullin3 E3 ligase, Sci. Adv. 9 (2023) eadg8369, https://doi.org/10.1126/sciadv.adg8369.

[18] H. Zuo, I. Glaaser, Y. Zhao, I. Kurinov, L. Mosyak, H. Wang, J. Liu, J. Park, A. Frangaj, E. Sturchler, M. Zhou, P. McDonald, Y. Geng, P.A. Slesinger, Q.R. Fan, Structural basis for auxiliary subunit KCTD16 regulation of the GABA $_B$ receptor, Proc. Natl. Acad. Sci. 116 (2019) 8370–8379, https://doi.org/10.1073/pnas.1903024116.

[19] D.M. Nguyen, D.H. Rath, D. Devost, D. Pétrin, R. Rizk, A.X. Ji, N. Narayanan, D. Yong, A. Zhai, D.A. Kuntz, M.U.Q. Mian, N.C. Pomroy, A.F.A. Keszei, S. Benlekbir, M.T. Mazhab-Jafari, J.L. Rubinstein, T.E. Hébert, G.G. Privé, Structure and dynamics of a pentameric KCTD5/CUL3/Gβγ E3 ubiquitin ligase complex, Proc. Natl. Acad. Sci. 121 (2024) e2315018121, https://doi.org/10.1073/pnas.2315018121.

[20] V. Sereikaite, T. Fritzius, V.B. Kasaragod, N. Bader, H.M. Maric, H. Schindelin, B. Bettler, K. Strømgaard, Targeting the γ-aminobutyric acid type B ($GABA_B$) receptor complex: development of inhibitors targeting the K^+ channel tetramerization domain (KCTD) containing proteins/GABA $_B$ receptor

protein–protein interaction, J. Med. Chem. 62 (2019) 8819–8830, https://doi.org/10.1021/acs.jmedchem.9b01087.
[21] L. Esposito, N. Balasco, G. Smaldone, R. Berisio, A. Ruggiero, L. Vitagliano, AlphaFold-predicted structures of KCTD proteins unravel previously undetected relationships among the members of the family, Biomolecules 11 (2021) 1862, https://doi.org/10.3390/biom11121862.
[22] L. Esposito, N. Balasco, L. Vitagliano, Alphafold predictions provide insights into the structural features of the functional oligomers of all members of the KCTD family, Int. J. Mol. Sci. 23 (2022) 13346, https://doi.org/10.3390/ijms232113346.
[23] N. Balasco, L. Esposito, G. Smaldone, M. Salvatore, L. Vitagliano, A comprehensive analysis of the structural recognition between KCTD proteins and Cullin 3, Int. J. Mol. Sci. 25 (2024) 1881, https://doi.org/10.3390/ijms25031881.
[24] G. Smaldone, L. Pirone, N. Balasco, S. Di Gaetano, E.M. Pedone, L. Vitagliano, Cullin 3 recognition is not a universal property among KCTD proteins, PLoS One 10 (2015) e0126808, https://doi.org/10.1371/journal.pone.0126808.
[25] N. Balasco, L. Pirone, G. Smaldone, S. Di Gaetano, L. Esposito, E.M. Pedone, L. Vitagliano, Molecular recognition of Cullin3 by KCTDs: insights from experimental and computational investigations, Biochim. Biophys. Acta BBA - Proteins Proteomics 2014 (1844) 1289–1298, https://doi.org/10.1016/j.bbapap.2014.04.006.
[26] J. Schwenk, M. Metz, G. Zolles, R. Turecek, T. Fritzius, W. Bildl, E. Tarusawa, A. Kulik, A. Unger, K. Ivankova, R. Seddik, J.Y. Tiao, M. Rajalu, J. Trojanova, V. Rohde, M. Gassmann, U. Schulte, B. Fakler, B. Bettler, Native GABAB receptors are heteromultimers with a family of auxiliary subunits, Nature 465 (2010) 231–235, https://doi.org/10.1038/nature08964.
[27] T. Fritzius, R. Turecek, R. Seddik, H. Kobayashi, J. Tiao, P.D. Rem, M. Metz, M. Kralikova, M. Bouvier, M. Gassmann, B. Bettler, KCTD hetero-oligomers confer unique kinetic properties on hippocampal GABA $_B$ receptor-induced K^+ currents, J. Neurosci. 37 (2017) 1162–1175, https://doi.org/10.1523/JNEUROSCI.2181-16.2016.
[28] D.C. Sloan, C.E. Cryan, B.S. Muntean, Multiple potassium channel tetramerization domain (KCTD) family members interact with Gβγ, with effects on cAMP signaling, J. Biol. Chem. 299 (2023) 102924, https://doi.org/10.1016/j.jbc.2023.102924.
[29] S. Dutta, I.B. Dawid, Kctd15 inhibits neural crest formation by attenuating Wnt/β-catenin signaling output, Development 137 (2010) 3013–3018, https://doi.org/10.1242/dev.047548.
[30] V.E. Zarelli, I.B. Dawid, Inhibition of neural crest formation by Kctd15 involves regulation of transcription factor AP-2, Proc. Natl. Acad. Sci. 110 (2013) 2870–2875, https://doi.org/10.1073/pnas.1300203110.
[31] L. Pirone, G. Smaldone, R. Spinelli, M. Barberisi, F. Beguinot, L. Vitagliano, C. Miele, S. Di Gaetano, G.A. Raciti, E. Pedone, KCTD1: a novel modulator of adipogenesis through the interaction with the transcription factor AP2α, Biochim. Biophys. Acta BBA - Mol. Cell Biol. Lipids 1864 (2019) 158514 https://doi.org/10.1016/j.bbalip.2019.08.010.
[32] the GIANT Consortium, Six new loci associated with body mass index highlight a neuronal influence on body weight regulation, Nat. Genet. 41 (2009) 25–34, https://doi.org/10.1038/ng.287.
[33] G. Smaldone, L. Pirone, A. Capolupo, L. Vitagliano, M.C. Monti, S. Di Gaetano, E. Pedone, The essential player in adipogenesis GRP78 is a novel KCTD15 interactor, Int. J. Biol. Macromol. 115 (2018) 469–475, https://doi.org/10.1016/j.ijbiomac.2018.04.078.
[34] A. Di Fiore, S. Bellardinelli, L. Pirone, R. Russo, A. Angrisani, G. Terriaca, M. Bowen, F. Bordin, Z.M. Besharat, G. Canettieri, F. Fabretti, S. Di Gaetano, L. Di Marcotullio, E. Pedone, M. Moretti, E. De Smaele, KCTD1 is a new modulator of the KCASH family of Hedgehog suppressors, Neoplasia 43 (2023) 100926, https://doi.org/10.1016/j.neo.2023.100926.
[35] L. Buono, C. Iside, G. Pecoraro, A. De Matteo, G. Beneduce, R. Penta De Vera d'Aragona, R. Parasole, P. Mirabelli, L. Vitagliano, M. Salvatore, G. Smaldone, A comprehensive analysis of the expression profiles of KCTD proteins in acute lymphoblastic leukemia: evidence of selective expression of KCTD1 in T-ALL, J. Clin. Med. 12 (2023) 3669, https://doi.org/10.3390/jcm12113669.
[36] G. Smaldone, L. Coppola, K. Pane, M. Franzese, G. Beneduce, R. Parasole, G. Menna, L. Vitagliano, M. Salvatore, P. Mirabelli, KCTD15 deregulation is associated with alterations of the NF-κB signaling in both pathological and physiological model systems, Sci. Rep. 11 (2021) 18237, https://doi.org/10.1038/s41598-021-97775-6.
[37] G. Smaldone, L. Coppola, M. Incoronato, R. Parasole, M. Ripaldi, L. Vitagliano, P. Mirabelli, M. Salvatore, KCTD15 protein expression in peripheral blood and acute myeloid leukemia, Diagnostics 10 (2020) 371, https://doi.org/10.3390/diagnostics10060371.
[38] G. Smaldone, G. Beneduce, M. Incoronato, K. Pane, M. Franzese, L. Coppola, A. Cordella, R. Parasole, M. Ripaldi, G. Nassa, A. Soricelli, L. Vitagliano, P. Mirabelli, M. Salvatore, KCTD15 is overexpressed in human childhood B-cell acute lymphoid leukemia, Sci. Rep. 9 (2019) 20108, https://doi.org/10.1038/s41598-019-56701-7.
[39] G. Smaldone, G. Pecoraro, K. Pane, M. Franzese, A. Ruggiero, L. Vitagliano, M. Salvatore, The oncosuppressive properties of KCTD1: its role in cell growth and mobility, Biology 12 (2023) 481, https://doi.org/10.3390/biology12030481.
[40] L. Coppola, S. Baselice, F. Messina, R. Giannatiempo, A. Farina, L. Vitagliano, G. Smaldone, M. Salvatore, KCTD15 is overexpressed in her2+ positive breast cancer patients and its silencing attenuates proliferation in SKBR3 CELL LINE, Diagnostics 12 (2022) 591, https://doi.org/10.3390/diagnostics12030591.
[41] G. Smaldone, N. Balasco, L. Pirone, D. Caruso, S. Di Gaetano, E.M. Pedone, L. Vitagliano, Molecular basis of the scalp-ear-nipple syndrome unraveled by the characterization of disease-causing KCTD1 mutants, Sci. Rep. 9 (2019) 10519, https://doi.org/10.1038/s41598-019-46911-4.
[42] L. Hu, L. Chen, L. Yang, Z. Ye, W. Huang, X. Li, Q. Liu, J. Qiu, X. Ding, KCTD1 mutants in scalp-ear-nipple syndrome and AP-2α P59A in Char syndrome reciprocally abrogate their interactions, but can regulate Wnt/β-catenin signaling, Mol. Med. Rep. (2020), https://doi.org/10.3892/mmr.2020.11457.
[43] L. Mazzarella, L. Vitagliano, A. Zagari, Swapping structural determinants of ribonucleases: an energetic analysis of the hinge peptide 16-22, Proc. Natl. Acad. Sci. 92 (1995) 3799–3803, https://doi.org/10.1073/pnas.92.9.3799.
[44] M.J. Bennett, S. Choe, D. Eisenberg, Domain swapping: entangling alliances between proteins, Proc. Natl. Acad. Sci. 91 (1994) 3127–3131, https://doi.org/10.1073/pnas.91.8.3127.
[45] K.K. Kojima, J. Jurka, Crypton transposons: identification of new diverse families and ancient domestication events, Mob. DNA 2 (2011) 12, https://doi.org/10.1186/1759-8753-2-12.
[46] P.D. Adams, P.V. Afonine, G. Bunkóczi, V.B. Chen, I.W. Davis, N. Echols, J. J. Headd, L.-W. Hung, G.J. Kapral, R.W. Grosse-Kunstleve, A.J. McCoy, N. W. Moriarty, R. Oeffner, R.J. Read, D.C. Richardson, J.S. Richardson, T. C. Terwilliger, P.H. Zwart, *PHENIX*: a comprehensive Python-based system for macromolecular structure solution, Acta Crystallogr. D Biol. Crystallogr. 66 (2010) 213–221, https://doi.org/10.1107/S0907444909052925.
[47] E. Potterton, P. Briggs, M. Turkenburg, E. Dodson, A graphical user interface to the *CCP* 4 program suite, Acta Crystallogr. D Biol. Crystallogr. 59 (2003) 1131–1137, https://doi.org/10.1107/S0907444903008126.
[48] A.A. Vagin, R.A. Steiner, A.A. Lebedev, L. Potterton, S. McNicholas, F. Long, G. N. Murshudov, *REFMAC* 5 dictionary: organization of prior chemical knowledge and guidelines for its use, Acta Crystallogr. D Biol. Crystallogr. 60 (2004) 2184–2195, https://doi.org/10.1107/S0907444904023510.
[49] P. Emsley, B. Lohkamp, W.G. Scott, K. Cowtan, Features and development of Coot, Acta Crystallogr. D Biol. Crystallogr. 66 (2010) 486–501, https://doi.org/10.1107/S0907444910007493.
[50] M. Gucwa, J. Lenkiewicz, H. Zheng, M. Cymborowski, D.R. Cooper, K. Murzyn, W. Minor, CMM—an enhanced platform for interactive validation of metal binding sites, Protein Sci. 32 (2023) e4525, https://doi.org/10.1002/pro.4525.
[51] N. Balasco, L. Esposito, L. Vitagliano, Factors affecting the amplitude of the τ angle in proteins: a revisitation, Acta Crystallogr. Sect. Struct. Biol. 73 (2017) 618–625, https://doi.org/10.1107/S2059798317007793.
[52] N. Balasco, L. Esposito, A.S. Thind, M.R. Guarracino, L. Vitagliano, Dissection of factors affecting the variability of the peptide bond geometry and planarity, Biomed. Res. Int. 2017 (2017) 1–9, https://doi.org/10.1155/2017/2617629.
[53] M. Mirdita, K. Schütze, Y. Moriwaki, L. Heo, S. Ovchinnikov, M. Steinegger, ColabFold: making protein folding accessible to all, Nat. Methods 19 (2022) 679–682, https://doi.org/10.1038/s41592-022-01488-1.
[54] D. Van Der Spoel, E. Lindahl, B. Hess, G. Groenhof, A.E. Mark, H.J.C. Berendsen, GROMACS: fast, flexible, and free, J. Comput. Chem. 26 (2005) 1701–1718, https://doi.org/10.1002/jcc.20291.
[55] T. Darden, D. York, L. Pedersen, Particle mesh Ewald: an *N*·log(*N*) method for Ewald sums in large systems, J. Chem. Phys. 98 (1993) 10089–10092, https://doi.org/10.1063/1.464397.
[56] B. Hess, H. Bekker, H.J.C. Berendsen, J.G.E.M. Fraaije, LINCS: a linear constraint solver for molecular simulations, J. Comput. Chem. 18 (1997) 1463–1472, https://doi.org/10.1002/(SICI)1096-987X(199709)18:12<1463::AID-JCC4>3.0.CO;2-H.
[57] W. Humphrey, A. Dalke, K. Schulten, VMD: visual molecular dynamics, J. Mol. Graph. 14 (1996) 33–38, https://doi.org/10.1016/0263-7855(96)00018-5.
[58] F. Rousseau, J. Schymkowitz, L.S. Itzhaki, Implications of 3D domain swapping for protein folding, misfolding and function, in: J.M. Matthews (Ed.), Protein Dimerization Oligomerization Biol, Springer New York, New York, NY, 2012, pp. 137–152, https://doi.org/10.1007/978-1-4614-3229-6_9.
[59] R. Berisio, S. Loguercio, A. De Simone, A. Zagari, L. Vitagliano, Polyproline helices in protein structures: a statistical survey, Protein Pept. Lett. 13 (2006) 847–854, https://doi.org/10.2174/092986606777841154.
[60] M.M. Harding, Geometry of metal–ligand interactions in proteins, Acta Crystallogr. D Biol. Crystallogr. 57 (2001) 401–411, https://doi.org/10.1107/S0907444900019168.
[61] F. Guo, D.N. Gopaul, G.D. Van Duyne, Asymmetric DNA bending in the Cre-*loxP* site-specific recombination synapse, Proc. Natl. Acad. Sci. 96 (1999) 7143–7148, https://doi.org/10.1073/pnas.96.13.7143.
[62] S. Barakat, E. Ezen, İ. Devecioğlu, M. Gezen, S. Piepoli, B. Erman, Dimerization choice and alternative functions of ZBTB transcription factors, FEBS J. 291 (2024) 237–255, https://doi.org/10.1111/febs.16905.
[63] P.M.C. Park, J. Park, J. Brown, M. Hunkeler, S.S. Roy Burman, K.A. Donovan, H. Yoon, R.P. Nowak, M. Słabicki, B.L. Ebert, E.S. Fischer, Polymerization of ZBTB transcription factors regulates chromatin occupancy, Mol. Cell 84 (2024) 2511–2524.e8, https://doi.org/10.1016/j.molcel.2024.06.010.
[64] L. Mance, N. Bigot, E. Zhamungui Sánchez, F. Coste, N. Martín-González, S. Zentout, M. Biliškov, Z. Pukało, A. Mishra, C. Chapuis, A.-A. Arteni, A. Lateur, S. Goffinont, V. Gaudon, I. Talhaoui, I. Casuso, M. Beaufour, N. Garnier, F. Artzner, M. Cadene, S. Huet, B. Castaing, M.J. Suskiewicz, Dynamic BTB-domain filaments promote clustering of ZBTB proteins, Mol. Cell 84 (2024) 2490–2510.e9, https://doi.org/10.1016/j.molcel.2024.05.029.
[65] A.G. Marneros, Aplasia cutis congenita pathomechanisms reveal key regulators of skin and skin appendage morphogenesis, J. Invest. Dermatol. (2024) S0022202X24017305, https://doi.org/10.1016/j.jid.2024.05.014.
[66] S. Su, R. Xie, X. Ding, Y. Lin, Three cases of bilateral breast absence associated with familial congenital ectodermal defects, Clin. Cosmet. Investig. Dermatol. 14 (2021) 377–383, https://doi.org/10.2147/CCID.S300010.

[67] S. Kumar, B. Rathkolb, S. Sabrautzki, S. Krebs, E. Kemter, L. Becker, J. Beckers, R. Bekeredjian, R. Brommage, J. Calzada-Wack, L. Garrett, S.M. Hölter, M. Horsch, M. Klingenspor, T. Klopstock, K. Moreth, F. Neff, J. Rozman, H. Fuchs, V. Gailus-Durner, M. Hrabe De Angelis, E. Wolf, B. Aigner, Standardized, systemic phenotypic analysis reveals kidney dysfunction as main alteration of Kctd1 I27N mutant mice, J. Biomed. Sci. 24 (2017) 57, https://doi.org/10.1186/s12929-017-0365-5.

[68] C. Ruangchan, C. Ngamphiw, A. Krasaesin, N. Intarak, S. Tongsima, M. Kaewgahya, K. Kawasaki, P. Mahawong, K. Paripurana, B. Sookawat, P. Jatooratthawichot, T.C. Cox, A. Ohazama, J.R. Ketudat Cairns, T. Porntaveetus, P. Kantaputra, Genetic variants in KCTD1 are associated with isolated dental anomalies, Int. J. Mol. Sci. 25 (2024) 5179, https://doi.org/10.3390/ijms25105179.

[69] J. Cheng, G. Novati, J. Pan, C. Bycroft, A. Žemgulytė, T. Applebaum, A. Pritzel, L. H. Wong, M. Zielinski, T. Sargeant, R.G. Schneider, A.W. Senior, J. Jumper, D. Hassabis, P. Kohli, Ž. Avsec, Accurate proteome-wide missense variant effect prediction with AlphaMissense, Science 381 (2023) eadg7492, https://doi.org/10.1126/science.adg7492.

[70] W. Makałowski, J. Zhang, M.S. Boguski, Comparative analysis of 1196 orthologous mouse and human full-length mRNA and protein sequences, Genome Res. 6 (1996) 846–857, https://doi.org/10.1101/gr.6.9.846.

[71] Z. Liu, F. Song, Z. Ma, Q. Xiong, J. Wang, D. Guo, G. Sun, Bivalent copper ions promote fibrillar aggregation of KCTD1 and induce cytotoxicity, Sci. Rep. 6 (2016) 32658, https://doi.org/10.1038/srep32658.

[72] R. Ebenhoch, S. Prinz, S. Kaltwasser, D.J. Mills, R. Meinecke, M. Rübbelke, D. Reinert, M. Bauer, L. Weixler, M. Zeeb, J. Vonck, H. Nar, A hybrid approach reveals the allosteric regulation of GTP cyclohydrolase I, Proc. Natl. Acad. Sci. 117 (2020) 31838–31849, https://doi.org/10.1073/pnas.2013473117.

[73] É.D. D'Andréa, Y. Roske, G.A.P.D. Oliveira, N. Cremer, A. Diehl, P. Schmieder, U. Heinemann, H. Oschkinat, J.R. Pires, Crystal structure of Q4D6Q6, a conserved kinetoplastid-specific protein from Trypanosoma cruzi, J. Struct. Biol. 211 (2020) 107536, https://doi.org/10.1016/j.jsb.2020.107536.

[74] L. Holm, DALI and the persistence of protein shape, Protein Sci. 29 (2020) 128–140, https://doi.org/10.1002/pro.3749.

[75] S. Kumar, M. Mazumder, N. Gupta, S. Chattopadhyay, S. Gourinath, Crystal structure of *Arabidopsis thaliana* calmodulin7 and insight into its mode of DNA binding, FEBS Lett. 590 (2016) 3029–3039, https://doi.org/10.1002/1873-3468.12349.

[76] B.S. Muntean, S. Marwari, X. Li, D.C. Sloan, B.D. Young, J.A. Wohlschlegel, K. A. Martemyanov, Members of the KCTD family are major regulators of cAMP signaling, Proc. Natl. Acad. Sci. 119 (2022) e2119237119, https://doi.org/10.1073/pnas.2119237119.